Ultrathin two-dimensional superconductivity with strong spin–orbit coupling

Hyoungdo Nam[a], Hua Chen[a], Tijiang Liu[b], Jisun Kim[a,1], Chendong Zhang[a], Jie Yong[c,2], Thomas R. Lemberger[c], Philip A. Kratz[d], John R. Kirtley[d], Kathryn Moler[d], Philip W. Adams[b], Allan H. MacDonald[a,3], and Chih-Kang Shih[a,3]

[a]Department of Physics, The University of Texas at Austin, Austin, TX 78712; [b]Department of Physics and Astronomy, Louisiana State University, Baton Rouge, LA 70803; [c]Department of Physics, The Ohio State University, Columbus, OH 43210; and [d]Department of Physics and Applied Physics, Stanford University, Stanford, CA 94305

Contributed by Allan H. MacDonald, July 29, 2016 (sent for review March 21, 2016; reviewed by Eva Y. Andrei and Laura Greene)

We report on a study of epitaxially grown ultrathin Pb films that are only a few atoms thick and have parallel critical magnetic fields much higher than the expected limit set by the interaction of electron spins with a magnetic field, that is, the Clogston–Chandrasekhar limit. The epitaxial thin films are classified as dirty-limit superconductors because their mean-free paths, which are limited by surface scattering, are smaller than their superconducting coherence lengths. The uniformity of superconductivity in these thin films is established by comparing scanning tunneling spectroscopy, scanning superconducting quantum interference device (SQUID) magnetometry, double-coil mutual inductance, and magneto-transport, data that provide average superfluid rigidity on length scales covering the range from microscopic to macroscopic. We argue that the survival of superconductivity at Zeeman energies much larger than the superconducting gap can be understood only as the consequence of strong spin–orbit coupling that, together with substrate-induced inversion-symmetry breaking, produces spin splitting in the normal-state energy bands that is much larger than the superconductor's energy gap.

superconductivity | ultrathin film | spin–orbit coupling | Zeeman | Rashba

Two-dimensional (2D) superconductivity is a topic of growing interest in contemporary condensed matter physics. Early experimental work in this field used granular thin films to study phase transitions to insulating normal states driven by weakened superfluid rigidity in the ultrathin film regime. Recent experimental progress (1–12) in epitaxial growth of uniform 2D superconductors whose properties are largely intrinsic has opened up new possibilities for the design of superconducting systems with specific desirable physical properties. Indeed, these almost ideal 2D systems have yielded (6, 12, 13) surprisingly robust superconductivity in films that are only one or two atomic layers thick, and very recently the observation of an astonishingly high T_c in single-layer FeSe on $SrTiO_3$ (14–17). In addition, because 2D superconductors must be placed on a substrate, they necessarily have broken inversion symmetry and Rashba-type spin–orbit interactions that break the spin degeneracy of quasiparticle levels in the normal state, and enable the possibility of achieving topological (18–21) superconducting states.

Here, we investigate the superconducting properties of strong spin–orbit coupling 2D superconductors using epitaxially grown, ultrathin Pb films on Si. By establishing that the superfluid rigidity vanishes at essentially the same T_c when measured on different length scales, from atomic to macroscopic (greater than millimeter), we demonstrate the uniformity of the superconductivity in our films and obtain highly reliable quantitative superfluid density (SFD) values. We then perform magneto-transport measurements in parallel fields, which clearly establish that the Clogston–Chandrasekhar (CC) limit does not apply to our films. Superconductivity at Zeeman fields well in excess of the superconducting energy gap can be understood only as a consequence of strong spin–orbit coupling that produces spin splitting in the normal-state energy bands that is much larger than the superconducting-state energy gap.

Results and Discussion

Fig. 1*A* shows scanning tunneling microscope (STM) images of a 5.0-monolayer (ML) (1.43 nm) film acquired at two different sample locations that are about 2 mm apart. The image in the *Inset* shows triangular pits covering about 1% of the surface area. These pits are five atomic layers deep, exposing very small wetting layer regions. The main STM image acquired at a location about 2 mm away shows that a further 1% of the surface is covered with additional 2D islands that are 2 ML thick. These observations affirm the thickness uniformity of the 5.0-ML film.

Scanning tunneling spectroscopy (STS) is used to measure the superconducting gap as a function of temperature (Fig. 1*B*). Bardeen–Cooper–Schrieffer (BCS)-like tunneling spectra with sharp coherence peaks at the quasiparticle band edges are clearly seen at 2.14 K. As the temperature is raised, the gap and the coherence peaks decrease. For the spectrum acquired at 6.57 K, the tunneling gap completely disappears, although a smooth but weak depression can be seen between ±10 mV. As reported previously, the weak-suppression feature persists at temperatures significantly above T_c (22, 23). The estimated superconducting gap values, Δ, are plotted as a function of T in Fig. 1*C* (red triangles). If we use data points with $\Delta > 0.5$ meV, the BCS fit yields a T_c of ∼5.9 K. However, we note that a small superconducting gap

Significance

By studying epitaxially grown Pb thin films, this paper explores a new regime in the physics of uniform 2D superconductivity, in which the spin–orbit coupling-induced Rashba splitting is larger than the superconducting gap. The first quantitative determination of superfluid rigidity in nearly atomically thin 2D superconductors was performed using measurement that covers microscopic to macroscopic length scales to establish uniformity. The extraordinarily strong parallel critical fields were discovered, which is greatly in excess of the normal Clogston–Chandrasekhar limit. Moreover, this remarkable behavior is theoretically explained as a consequence of strong spin–orbit coupling in 2D superconductors that are uniform but in the dirty limit.

Author contributions: H.N., H.C., T.R.L., J.R.K., K.M., P.W.A., A.H.M., and C.-K.S. designed research; H.N., H.C., T.L., J.K., C.Z., J.Y., T.R.L., P.A.K., J.R.K., K.M., P.W.A., A.H.M., and C.-K.S. performed research; H.N., H.C., T.L., J.K., C.Z., J.Y., T.R.L., P.A.K., J.R.K., K.M., P.W.A., A.H.M., and C.-K.S. analyzed data; and H.N., H.C., T.R.L., J.R.K., K.M., P.W.A., A.H.M., and C.-K.S. wrote the paper.

Reviewers: E.Y.A., Rutgers; and L.G., National Magnet Lab.

The authors declare no conflict of interest.

Freely available online through the PNAS open access option.

[1]Present address: Department of Physics and Astronomy, Louisiana State University, Baton Rouge, LA 70803.

[2]Present address: Department of Physics, University of Maryland, College Park, MD 20742.

[3]To whom correspondence may be addressed. Email: macd@physics.utexas.edu or shih@physics.utexas.edu.

This article contains supporting information online at www.pnas.org/lookup/suppl/doi:10.1073/pnas.1611967113/-/DCSupplemental.

PHYSICS

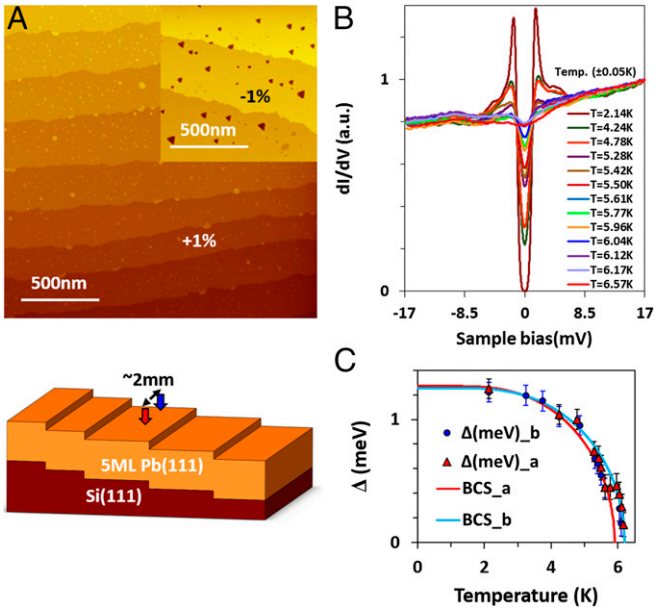

Fig. 1. STS measurement of superconductivity of a 5-ML Pb film. (*A*) STM images of a 5-ML MBE-grown Pb(111) film on a Si(111) substrate acquired at two different locations that are 2 mm apart, showing that the uniformity of the film coverage is about ±1%. (*B*) STS measured at different sample temperatures. (*C*) Two sets of superconducting gap values as a function of temperature were taken at different locations on the same sample with different tips, respectively. Each superconducting gap value was obtained by fitting the normalized differential conductance to the BCS theory density of states. Two BCS fits are shown as solid lines with red curve labeling the fit using only data points with $\Delta > 0.5$ meV ($T_c = 5.9$ K) and the light blue curve fit including all small gap data points.

persists above this T_c value, which can also be seen directly in the original tunneling spectra shown in Fig. 1*B*. This deviation from the smooth BCS fit has been reproduced with different tips and different 5-ML films. We note that, in a recent STM investigation of 3D Pb nanodots (24), a similar break from the smooth BCS fit has also been observed. In the 2D ultrathin film case reported here, however, the temperature region where the deviation is observed is rather narrow. This intriguing phenomenon warrants further investigation, but is outside the scope of the current paper.

After capping this 5-ML film with 3 nm of amorphous Ge in the molecular beam epitaxy (MBE) system, the film is removed for macroscopic and mesoscopic measurements using ex situ double-coil measurements (millimeter scale) and scanning superconducting quantum interference device (SQUID) magnetometry (SSM) (micrometer scale). Both techniques measure the mutual inductance between two coils from which the penetration depth is deduced. In Fig. 2*A*, we show the atomic force microscope (AFM) image of the measured capped film. The corresponding STM image, measured in a similar area before capping, is shown as the *Inset* to Fig. 1*A*. Note that, in this region, the coverage is about 1% deficient as revealed by STM. This morphology is replicated after Ge capping, reflecting the atomic smoothness of Ge capping film. We emphasize that the quality of Ge capping is extremely important to obtain reliable ex situ superconductivity measurements. Less uniform Ge capping (judged by a rougher surface in the AFM image) disrupts the integrity of the ultrathin Pb film, leading to significant suppression (or total loss) of superconductivity.

In double-coil measurements, it is conventional to express $n_s(T)$ in terms of the magnetic penetration depth, λ, because $n_s(T) \propto 1/\lambda^2(T)$. The T dependence of λ^{-2} (Fig. 2*B*) is unusual in that there is a long steep drop to zero at T_c that will be discussed elsewhere. Here, we want to emphasize that T_c is about 5.75 K, whether it is defined from the peak in σ_1 (*Methods*) or from the intersection of the Berezinskii–Kosterlitz–Thouless (BKT) theory (25, 26) line ($\lambda^{-2} = 8\pi\mu_0 k_B T/d\Phi_0^2$) with the data. Here, μ_0 is the magnetic permeability of vacuum, d is the film thickness, Φ_0 is the superconducting flux quantum, and k_B is the Boltzmann constant. The T_c value is very close to the value determined by using STS, a local probe, confirming that the gap and phase rigidity are consistent across the millimeter-scale breadth of our films. (If the phase rigidity is large compared with the gap, the transition temperature is determined by the gap. However, when the phase rigidity is similar to gap, phase fluctuations play a large role in superconductivity. Indeed, in this regime the superconducting properties cannot be adequately described by mean-field-theory. A detailed description of the relation between gap and phase rigidity can be found in ref. 27.) The robustness of phase rigidity is further confirmed by the sharp transition observed in the transport study discussed below. The SFD value observed in this 5-ML film is only ~5/μm^2, about 130 times lower than the SFD of bulk Pb in the clean limit, ~650/μm^2. [The canonical penetration depth in pure bulk Pb is $\lambda_0 = 39$ nm (28).] A reduction of about this size is expected because normal state resistivity and perpendicular critical field measurements (see below) show that the elastic mean free path (mfp) ℓ in our films is about equal to the film thickness, and is therefore about 60 times shorter than the canonical bulk coherence length in Pb, $\xi \sim 80$ nm (28). In "dirty" superconductors, the SFD is reduced by ℓ/ξ. We note, however, that the diameter of the coils used in this measurement is comparable to the width of our samples (about 3 mm) and that geometrical effects might therefore lead to a slight underestimate of the SFD.

However, even the reduced SFD implies a phase rigidity energy scale (27)

$$V_0 = \frac{(\hbar c)^2 d}{16\sqrt{\pi} e^2 \lambda^2(0)},$$

where d is the film thickness, that is much larger than the measured critical temperature. For example, when $\lambda^{-2}(0) = 5/\mu m^2$ and $d = 1.43$ nm, we obtain $V_0/k_B \sim 80\ K \gg T_c$. Although the

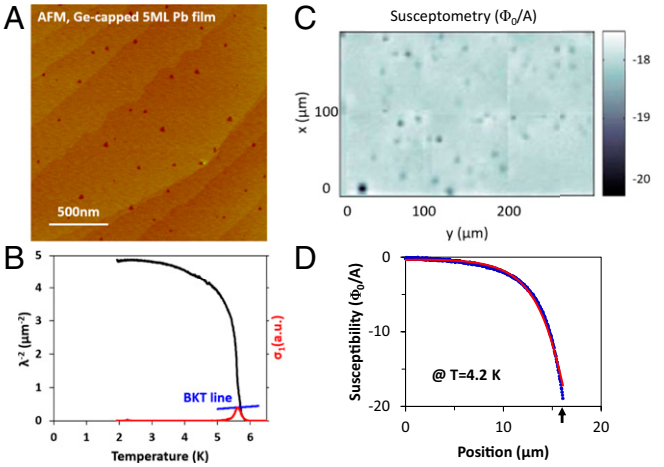

Fig. 2. Ex situ double-coil and scanning-SQUID measurements of a Ge-capped 5-ML Pb film. (*A*) AFM image of 5-ML Pb film after Ge capping (3 nm). (*B*) Temperature-dependent SFD measured on the Ge-capped sample at a frequency of 50 kHz (black) using double-coil measurements. The red curve is the real part of the film complex conductivity and the intersection between "BKT line" and SFD curve predicts BKT transition temperature. (*C*) Susceptometry image at $T = 4.2$ K in a magnetic field less than 0.3 μT using scanning-SQUID. (*D*) SQUID susceptibility measurements as a function of the height of the SQUID sensor. The touchdown position is of 16 μm, marked by an arrow. The solid line is a fit of data to an SQUID susceptibility expression for a uniform, thin diamagnetic sample, using the Pearl length Λ as a fitting parameter.

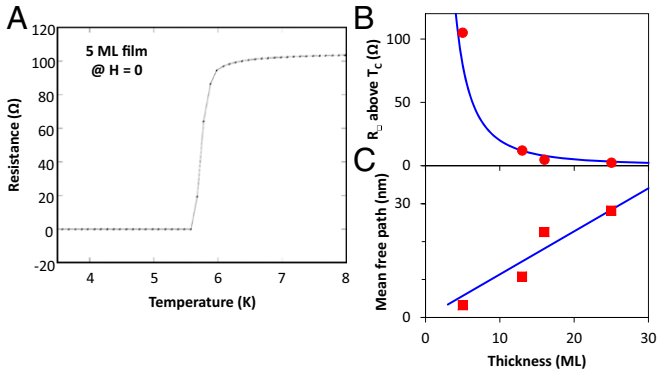

Fig. 3. Transport measurements at $H = 0$ on Ge-capped thin Pb films. (*A*) *R*–*T* of 5-ML Pb film with a clean superconducting transition at $T = 5.75$ K and a low normal-state sheet resistance of ∼100 Ω ($<<h/4e^2$). (*B*) Normal-state sheet resistances following $1/d^2$ dependence, where *d* is the film thickness. (*C*) The mfp showing a linear dependence on *d*.

SFD is reduced, we expect phase rigidity to survive up to close to the mean-field transition temperature, as confirmed by the similar T_c observed between STS and double-coil measurements.

To investigate superconducting properties at a mesoscopic length scale, the same sample (5-ML epitaxial Pb film capped with 3-nm Ge) was probed using SSM with a pickup loop 3 μm in diameter, and a field coil with an effective radius of $a = 8.4$ μm. Fig. 2*C* shows the variation in SQUID susceptibility, phase sensitively sensing the magnetic flux through the pickup loop due to a 98-μA amplitude ac current through the field coil. This image was acquired at a tip-sample separation of 2 μm at $T = 4.2$ K. Almost constant susceptibility reflects uniform superconductivity on the whole sample area, except for black dots (∼8 dots per 100 μm × 100 μm).

Fig. 2*D* shows the susceptibility touchdown at $T = 4.2$ K. The dots are the data acquired as a function of the height, *z*, of the tip above the film, and the solid line is a fit to the SQUID susceptibility expression for a thin diamagnetic film from which a Pearl length Λ of ∼110 μm is obtained (details described in *Methods*). If we assume uniform film thickness, the Pearl length is directly related to the SFD measured using the double-coil experiment using $\Lambda = 2\lambda^2/d$. Taking $d = 1.43$ nm, a SFD of 13/μm^2 at 4.2 K is obtained, compared with 4.5/μm^2, the double-coil measurement value at this temperature. The factor of 2–3 difference is partially explained by the finite-sample size effect in the double-coil measurement mentioned above. From the temperature dependence of $1/\Lambda$, one can estimate again that T_c is somewhere between 5.5 K and 6 K (*SI Appendix*, Fig. S3). If a SFD of 13/μm^2 is used, then the phase rigidity is even higher with $V_0/k_B \sim 210$ K.

We emphasize that these three measurements probe superconductivity on dramatically different length scales, spanning seven orders of magnitude from angstroms to millimeters. All give consistent values for T_c, attesting to the superconducting phase rigidity across the entire area of ultrathin superconducting films that are only a few atoms thick. The measured SFDs are also rather consistent at different length scales (micrometer for SSM and millimeter for double coils).

Fig. 3*A* plots resistance vs. temperature (*R*–*T*) for a 5-ML Ge-capped film. A very sharp superconducting transition is observed at 5.75 K, close to the T_c values inferred from the STM and SFD measurements described above. The sharpness of the transition contrasts markedly with the behavior reported for nonuniform ultrathin superconducting films that have much lower areal superfluid densities, allowing phase fluctuation physics to broaden the resistive transition. The normal-state sheet resistance R_s is ∼105 Ω, which is two orders of magnitude lower than the quantum resistance $h/4e^2 \approx 6.5$ kΩ, confirming that quantum fluctuations do not have a large influence on the transition temperature (27). From the sheet resistance and the free-electron model (29), one can estimate a carrier relaxation time of 1.9 fs $[\tau = (0.22/R_s d)(r_s/a_0)^3 \times 10^{-14}\ \mu\Omega\cdot\text{cm}\cdot\text{s}]$ and a mfp of 3.2 nm $[\ell = (1/R_s d)(r_s/a_0)^2 \times 9.2\ \mu\Omega\cdot\text{cm}\cdot\text{nm}]$, roughly twice the film thickness. Here, $r_s/a_0 = 2.3$ for Pb, where r_s is the effective radius of a sphere whose volume is equal to the volume per conduction electron, and a_0 is Bohr radius (29). A corroborating estimate of mfp comes from the perpendicular critical field, $H_{c\perp}(2\text{K}) = 1.56$ T and 0.63 T for 5- and 13-ML films (Fig. 4 *C* and *D*), interpreted using the pair breaking theory of Maki and Tinkham (details described in *SI Appendix*, section 3), and an experimental Fermi velocity v_F of 1.0×10^6 m/s (30). (Note, the experimental v_F from ref. 30 was used for more practical estimation of mfp, instead of the ideal v_F induced from electron density of a material in free-electron model). This method yields mfp values of 0.8 nm and 2.4 nm, respectively, again comparable to film thickness. Moreover, measurements at different thicknesses show that the sheet resistance roughly scales as $1/d^2$ (Fig. 3*B*), implying that the mfp scales linearly with *d* (Fig. 3*C*). This indicates that surface scattering dominates normal-state transport. This scaling behavior has been observed in other epitaxial thin films that are free of grain boundary scattering.

Fig. 4*A* illustrates the resistive transition of the 5-ML film as a function of parallel magnetic field. Most interestingly, T_c changes only slightly even at a parallel magnetic field of 9 T, the highest field we studied. Because T_c decreases roughly linearly with field (*SI Appendix*, Fig. S4), we extrapolate to a zero-temperature critical field in the range of 50 T. Pair breaking due to the Zeeman energy in the low-spin–orbit scattering regime is predicted to be linear in *H* (31) and to extrapolate to a $T = 0$ critical field of $\Delta/(\sqrt{2}\mu_B)$. Using $\Delta = 1.23$ meV from Fig. 1*C*, we obtain a critical Zeeman field of about 15 T. Clearly, the Zeeman effect is greatly reduced, and we argue below that it is reduced by strong spin–orbit scattering, which make the Zeeman pair-breaking effect quadratic in field. The observed linear reduction in T_c with magnetic field might be due to substrate surface steps, which make it impossible to achieve perfect parallel alignment globally and therefore to fully eliminate the strong orbital coupling effect associated with perpendicular components of the magnetic field.

Field angle-dependent *R* vs. *H* measurements at a constant temperature of 2 K have also been carried out (Fig. 4 *C* and *D*). Note that the critical field gradually increases as the angle is decreased. Below 6°, the critical field could not be reached at the maximum magnetic field (9 T) of our measurement system. In the case of the 13-ML film, which has a perpendicular critical field of 0.63 T, the critical field at 2° is estimated to be ∼10.25 T. Using the Tinkham equation (32) to fit $H_c(\theta)$ requires data points at small angles that are available only for the 13-ML film. The fit yields $H_{c\parallel}$ of ∼16 T at 2 K for the 13-ML film (Fig. 4*E*). We note that, for $\theta > 10°$, the critical field at 5 ML is about 2.5 times higher than that of the 13-ML sample, allowing us to estimate that $H_{c\parallel} \sim$ at least 40 T at 2 K for the 5-ML film, which greatly exceeds the CC limit of 15 T.

Experimentally, this behavior is consistent with a picture that the pair breaking is dominated by the orbital effect. Let us consider the pair-breaking orbital effect, in parallel field $\alpha_o = (\hbar/6)(D\pi^2/\Phi_0^2)H_\parallel^2 d^2$, and in perpendicular field this becomes $\alpha_o = (\hbar D\pi/\Phi_0)H_{c\perp}$, where *D* is the diffusion coefficient, Φ_0 is the quantum flux, and *d* is the film thickness. Provided that the orbital effect is the only contribution to the pair breaking, there is a simple relationship between $H_{c\parallel}$ and $H_{c\perp}$ as follows:

$$H_{c\perp} = \frac{\pi}{6}\frac{d^2}{\Phi_0}H_{c\parallel}^2.$$

Using this expression and the measured $H_{c\perp}(2\text{ K})$ of 1.56 and 0.63 T for 5 ML and 13 ML, we derive $H_{c\parallel}(2\text{ K})$ of 54.9 and 13.6 T, respectively, values very close to the angular fit using Tinkham

PHYSICS

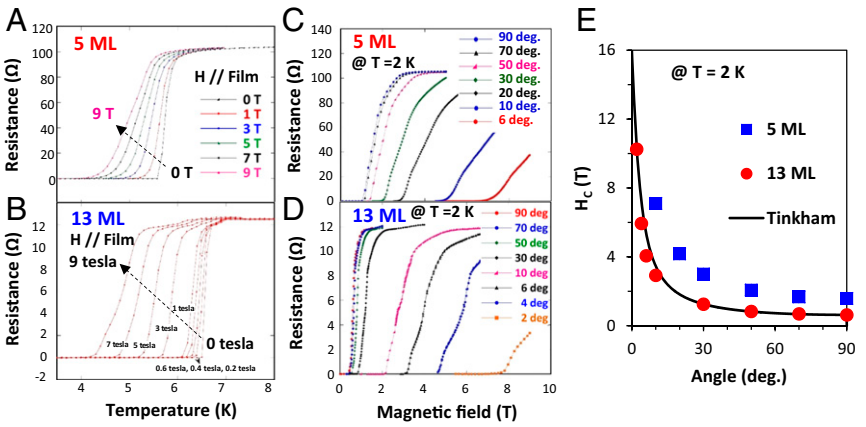

Fig. 4. Magnetotransport measurements. (*A* and *B*) *R–T* measurements as a function of magnetic field in parallel geometry for 5-ML film (*A*) and 13-ML film (*B*), respectively. (*C* and *D*) Angular-dependent *R–H* measurement at $T = 2$ K for 5-ML film (*C*) and 13-ML film (*D*), respectively. (*E*) Angle-dependent critical field $H_c(\theta)$, for 5-ML (blue) and for 13-ML (red) films. Tinkham formula fit (black) to 13-ML data at $T = 2$ K indicates a parallel critical field of $H_{c\|} = 16$ T.

formula. Thus, experimentally, we establish that in this ultrathin film system, the pair breaking is primarily orbital effect even in the field strength far exceeding CC limit.

The extraordinarily high parallel critical field is due to the large atomic spin–orbit coupling of Pb and to broken inversion symmetry at the film surface. The effects of spin–orbit splitting of the quasiparticle bands can be qualitatively understood by considering a 2D electron gas model with Rashba spin–orbit coupling and *s*-wave superconductivity pairing (33). In the limit that the spin–orbit splitting energy is large, $E_{so} \gg \hbar/\tau \gg \Delta$, the conduction band splits into Rashba subbands and the spin direction is locked to the momentum direction. It follows that spin-independent scattering between different band momenta will suppress normal state spin-polarization and therefore the pair-breaking effects of an external Zeeman field. Indeed, in the strong spin–orbit coupling limit, the Zeeman pair-breaking parameter $\alpha_s = 2(\mu_B H)^2\tau/\hbar$ (ref. 34 and *SI Appendix*, section 6) gives a critical field exceeding the CC limit by a factor of $1/\sqrt{2\Delta(0)\tau/\hbar} \sim 12$ for the 5-ML film ($\tau \sim 1.9$ fs estimated from transport measurements in the normal state of the Pb films), a value consistent with the experimental observation.

It is normally assumed that, in ultrathin superconducting films with a thickness d that is much smaller than the coherence length ξ, the orbital pair-breaking effect of the parallel field ($\alpha_o = e^2 v_F^2 d^2 H^2 \tau/18\hbar$) is quenched and the spin pair-breaking effect is dominant. However, in the present system, the spin pair-breaking effect is so strongly suppressed by the spin–orbit coupling and impurity scattering, that even for our 5-ML film the spin effect α_s is smaller than the orbital effect α_o by a factor of ~50. In other words, the theoretical critical parallel field is completely dominated by the orbital rather than the spin pair-breaking channel, and is estimated to be about 56 T for the 5-ML film. The quenching of the spin degrees of freedom in strong spin–orbit coupling systems makes them poor candidates for observance of the Fulde–Ferrell–Larkin–Ovchinnikov phase (35, 36).

Another very interesting aspect of our observations is the increase with parallel magnetic field of the width in temperature of the resistive superconducting transition. For the 5-ML film, the transition width changes from 0.2 K at zero field, to about 0.85 K at 9 T (from 10% to 90% of the normal-state resistance). For the 13-ML film, this broadening of the transition width is about 0.7 K at 9 T. Measurements carried out on other thicknesses show consistent behavior: the parallel critical field decreases as the thickness increases, but the broadening of the transition width at high field is also smaller. We can exclude the possibility that the SFD is strongly reduced by the parallel field based on theoretical considerations, so the broadening is not due to enhanced phase fluctuations (*SI Appendix*, section 7). We ascribe the broadening instead to inhomogeneity due to the presence of substrate step edges that lead to scattering time τ variation on a length scale ζ which is much larger than the mfp. This type of inhomogeneity does not influence T_c in the absence of magnetic fields (37), but will lead to spatial variation of T_c when the field is nonzero, because both pair-breaking parameters, α_s and α_o, depend on τ. The fact that the broadening is less pronounced in thicker films can also be understood in this way because substrate steps will play a weaker role. In this interpretation, the broadened transition width corresponds to a percolative superconducting-normal transition (38).

In summary, our work shows that MBE-grown ultrathin metallic films can have superfluid densities that are large enough that phase fluctuations have little effect on critical temperatures. Furthermore, we find that two features that we expect to be rather common in ultrathin metal films: (*i*) mfps that are limited to the film thickness by scattering from the surface or the interface with the substrate, and drive the superconductivity into the dirty limit; and (*ii*) strong spin–orbit scattering because of broken inversion symmetry. Together, these properties conspire to produce enormously large in-plane critical magnetic fields. The giant critical magnetic fields, combined with the superior crystalline quality and the strong spin–orbit coupling, make ultrathin Pb films an intriguing platform for tuning the strength of time-reversal symmetry breaking in a superconducting state, and realizing topological superconductors that are relevant for quantum computation.

Methods

The ultrathin Pb films are grown using MBE on Si(111) substrates. Before film growth, the Si surface is prepared to create a dense-phase $\sqrt{3}\times\sqrt{7}$ Pb/Si(111) reconstruction (39, 40) as the template. Epitaxial Pb(111) films are grown using a two-step process described previously—low-temperature deposition at 80 K, followed by room temperature annealing (41). The double-coil experiment determines the SFD, a measure of condensate rigidity in superconducting films, from the mutual inductance of coaxial coils located on opposite sides of the sample film (10, 42). Basically, induced supercurrents attenuate and shift the phase of the mutual inductance by an amount determined by the complex sheet conductivity, $(\sigma_1 + i\sigma_2)d$, of the film. The areal density, $n_s(T)d$, of superconducting electrons is proportional to $\sigma_2 d$. The frequency of ac current in the drive coil in our experiment was 50 kHz. Coil diameters are typically about a millimeter, so the experiment probes at the macro level. In Fig. 2*D*, the solid line is a fit to the SQUID susceptibility expression for a thin diamagnetic film, $\phi(z)/\phi_s = (-a/\Lambda)(1 - 2\bar{z}/\sqrt{1+4\bar{z}^2})$, $\phi(z) \equiv \Phi(z)/I\Phi_0$, where $\Phi(z)$ is the flux through the pickup loop, I is the current through the field coil, and $\bar{z} = z/a$, using the Pearl length, Λ, as a fitting parameter (43). Taking $a = 8.4$ μm, the sensor self-inductance $\phi_s = 800$ 1/A, and

estimating a minimum height of the SQUID pickup loop above the sample surface $z_0 = 2.5$ μm, we obtain the Pearl length of ∼110 μm.

ACKNOWLEDGMENTS. Film growth and STM measurements performed at The University of Texas at Austin were supported by Office of Naval Research Grant ONR-N00014-14-1-0330, Welch Foundation Grant F-1672, and National Science Foundation (NSF) Grant DMR-1506678. Double-coil measurements performed at The Ohio State University were supported by US Department of Energy , Office of Science, Basic Energy Sciences, through Grant FG02-08ER46533. Magnetotransport measurements were performed at Louisiana State University via the support of the US Department of Energy, Office of Science, Basic Energy Sciences, under Award DE-FG02- 07ER46420. The SQUID microscope used in this work was developed with the support of an NSF Instrumentation for Materials Research–Major Instrumentation Projects contract, Award 0957616. J.K. was supported under the auspices of an NSF Nanoscale Science and Engineering Center: Center for Probing the Nanoscale, Award 0425897. Work by J.R.K., P.A.K., and K.M. was supported by the Department of Energy, Office of Science, Basic Energy Sciences, Materials Sciences and Engineering Division, under Contract DE-AC02-76SF00515. H.C. and A.H.M. were supported by Office of Naval Research Grant ONR-N00014-14-1-0330 and Welch Foundation Grant TBF1473.

1. Guo Y, et al. (2004) Superconductivity modulated by quantum size effects. *Science* 306(5703):1915–1917.
2. Ozer MM, Thompson JR, Weitering HH (2006) Hard superconductivity of a soft metal in the quantum regime. *Nat Phys* 2(3):173–176.
3. Eom D, Qin S, Chou MY, Shih CK (2006) Persistent superconductivity in ultrathin Pb films: A scanning tunneling spectroscopy study. *Phys Rev Lett* 96(2):027005.
4. Ozer MM, Jia Y, Zhang Z, Thompson JR, Weitering HH (2007) Tuning the quantum stability and superconductivity of ultrathin metal alloys. *Science* 316(5831):1594–1597.
5. Nishio T, et al. (2008) Superconducting Pb island nanostructures studied by scanning tunneling microscopy and spectroscopy. *Phys Rev Lett* 101(16):167001.
6. Qin S, Kim J, Niu Q, Shih CK (2009) Superconductivity at the two-dimensional limit. *Science* 324(5932):1314–1317.
7. Kim J, et al. (2012) Visualization of geometric influences on proximity effects in heterogeneous superconductor thin films. *Nat Phys* 8(6):464–469.
8. Yoshii K, Yamamoto H, Saiki K, Koma A (1995) Superconductivity and electrical properties in single-crystalline ultrathin Nb films grown by molecular-beam epitaxy. *Phys Rev B Condens Matter* 52(18):13570–13575.
9. Mondal M, et al. (2011) Role of the vortex-core energy on the Berezinskii–Kosterlitz–Thouless transition in thin films of NbN. *Phys Rev Lett* 107(21):217003.
10. Yong J, et al. (2013) Robustness of the Berenzinskii–Kosterlitz–Thouless transition in ultrathin NbN films near the superconductor-insulator transition. *Phys Rev B* 87(18): 184505.
11. Xing Y, et al. (2015) Quantum Griffiths singularity of superconductor-metal transition in Ga thin films. *Science* 350(6260):542–545.
12. Uchihashi T, Mishra P, Aono M, Nakayama T (2011) Macroscopic superconducting current through a silicon surface reconstruction with indium adatoms: Si(111)-($\sqrt{7} \times \sqrt{3}$)-In. *Phys Rev Lett* 107(20):207001.
13. Zhang T, et al. (2010) Superconductivity in one-atomic-layer metal films grown on Si (111). *Nat Phys* 6(2):104–108.
14. Wang QY, et al. (2012) Interface-induced high-temperature superconductivity in single unit-cell FeSe films on $SrTiO_3$. *Chin Phys Lett* 29(3):037402.
15. Liu D, et al. (2012) Electronic origin of high-temperature superconductivity in single-layer FeSe superconductor. *Nat Commun* 3:931.
16. Tan S, et al. (2013) Interface-induced superconductivity and strain-dependent spin density waves in FeSe/$SrTiO_3$ thin films. *Nat Mater* 12(7):634–640.
17. Ge JF, et al. (2015) Superconductivity above 100 K in single-layer FeSe films on doped SrTiO3. *Nat Mater* 14(3):285–289.
18. Fu L, Berg E (2010) Odd-parity topological superconductors: Theory and application to CuxBi2Se3. *Phys Rev Lett* 105(9):097001.
19. Qi XL, Zhang SC (2011) Topological insulators and superconductors. *Rev Mod Phys* 83(4):1057–1110.
20. Wang J, Xu Y, Zhang SC (2014) Two-dimensional time-reversal-invraiant topological superconductivity in a doped quantum spin-Hall insulator. *Phys Rev B* 90(5):054503.
21. Hao N, Shen SQ (2015) Topological superconducting states in monolayer FeSe/$SrTiO_3$. *Phys Rev B* 92(16):165104.
22. Wang K, Zhang X, Loy MM, Chiang TC, Xiao X (2009) Pseudogap mediated by quantum-size effects in lead islands. *Phys Rev Lett* 102(7):076801.
23. Kim J, et al. (2011) Universal quenching of the superconducting state of two-dimensional nanosize Pb-island structures. *Phys Rev B* 84(1):014517.
24. Brihuega I, et al. (2011) Experimental observation of thermal fluctuations in single superconducting Pb nanoparticles through tunneling measurements. *Phys Rev B* 84(10):104525.
25. Kosterlitz JM, Thouless DJ (1973) Ordering metastability and phase transitions in two-dimensional system. *J Phys Chem* 6(7):1181–1203.
26. Chaikin PM, Lubensky TC (1995) Topological defects. *Principles of Condensed Matter Physics* (Cambrige Univ Press, New York), pp 495–589.
27. Emery VJ, Kivelson SA (1995) Importance of phase fluctuations in superconductors with small superfluid density. *Nature* 374(6521):434–437.
28. Meservey R, Schwartz BB (1969) Equilibrium protperites: Comparsion of experimental results with predictions of the BCS theory. *Superconductivity*, ed Parks RD (Marcel Dekker, New York), Vol I, pp 117–191.
29. Ashcroft NW, Mermin ND (1976) The Sommerfeld thoery of metals. *Solid State Physics* (Holt, Rinehart and Winston, New York), pp 29–55.
30. Lykken GI, Geiger AL, Mitchell EN (1970) Measurement of the Fermi velocity in single-crystal films of lead by electron tunneling. *Phys Rev Lett* 25(22):1578–1580.
31. Tinkham M (2004) Special topics. *Introduction to Superconductivity* (Dover Publications, New York), pp 384–402.
32. Tinkham M (1963) Effect of fluxoid quantization on transitions of superconducting films. *Phys Rev* 129(6):2413–2422.
33. Gor'kov LP, Rashba EI (2001) Superconducting 2D system with lifted spin degeneracy: Mixed singlet-triplet state. *Phys Rev Lett* 87(3):037004.
34. Dimitrova O, Feigel'man MV (2007) Theory of a two-dimensional superconductor with broken inversion symmetry. *Phys Rev B* 76(1):014522.
35. Fulde P, Ferrell RA (1964) Superconductivity in a strong spin-exchange field. *Phys Rev* 135(3A):A550–A563.
36. Larkin AI, Ovchinnikov YN (1964) Nonuniform state of superconductors. *Zh Eksp Teor Fiz* 47(3):1136–1146.
37. Anderson PW (1959) Theory of dirty superconductors. *J Phys Chem Solids* 11(1-2): 26–30.
38. Ioffe LB, Larkin AL (1981) Properties of superconductors with a smeared transition temperature. *Zh Eksp Teor Fiz* 81(2):707–718.
39. Hupalo M, Schmalian J, Tringides MC (2003) "Devil's staircase" in Pb/Si(111) ordered phases. *Phys Rev Lett* 90(21):216106.
40. Lu SM, et al. (2012) Scanning tunneling spectroscopy observation of electronic resonances originating from 1×1 potential on the dense Pb overlayer on Si(111). *Jpn J Appl Phys* 51(1R):015702.
41. Smith AR, Chao KJ, Niu Q, Shih CK (1996) Formation of atomically flat silver films on GaAs with a "silver mean" quasi periodicity. *Science* 273(5272):226–228.
42. Hetel I, Lemberger TR, Randeria M (2007) Quantum critical behaviour in the superfluid density of strongly underdoped ultrathin copper oxide films. *Nat Phys* 3(10): 700–702.
43. Kirtley JR, et al. (2012) Scanning SQUID susceptometry of a paramagnetic superconductor. *Phys Rev B* 85(22):224518.